AIP | Applied Physics Letters

High efficiency InGaN/GaN light emitting diodes with asymmetric triangular multiple quantum wells

Chiao-Yun Chang, Hen Li, and Tien-Chang Lu

Citation: Applied Physics Letters **104**, 091111 (2014); doi: 10.1063/1.4867023
View online: http://dx.doi.org/10.1063/1.4867023
View Table of Contents: http://scitation.aip.org/content/aip/journal/apl/104/9?ver=pdfcov
Published by the AIP Publishing

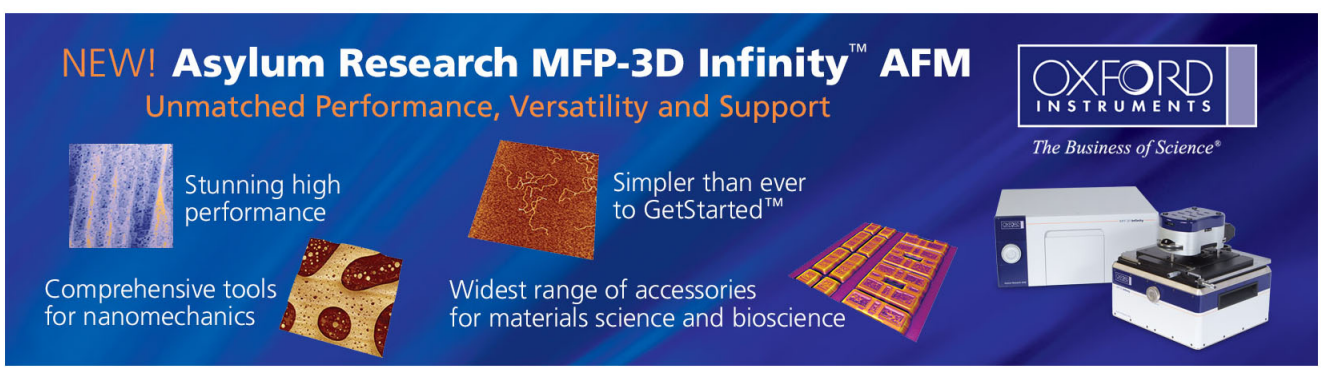

High efficiency InGaN/GaN light emitting diodes with asymmetric triangular multiple quantum wells

Chiao-Yun Chang, Hen Li, and Tien-Chang Lu[a)]
Department of Photonics and Institute of Electro-Optical Engineering, National Chiao Tung University, 1001 University Road, Hsinchu, Taiwan 300, Republic of China

(Received 19 November 2013; accepted 14 February 2014; published online 4 March 2014)

In this study, we demonstrated high efficiency InGaN/GaN light emitting diodes (LEDs) with asymmetric triangular multiple quantum wells (MQWs). Asymmetric triangular MQWs not only contribute to uniform carrier distribution in InGaN/GaN MQWs but also yield a low Auger recombination rate. In addition, asymmetric triangular MQWs with gallium face-oriented inclination band profiles can be immune from the polarization charge originating from typical c-plane InGaN/GaN quantum well structures. In the experiment, LEDs incorporated with asymmetric triangular MQWs with gallium face-oriented inclination band profiles exhibited a 60.0% external quantum efficiency at 20 mA and a 27.0% efficiency droop at 100 mA (corresponding to a current density of 69 A/cm^2), which accounted for an 11.7% efficiency improvement and a 31.1% droop reduction compared with symmetric square quantum well structure LEDs. © *2014 AIP Publishing LLC*. [http://dx.doi.org/10.1063/1.4867023]

Recently, InGaN/GaN light emitting diodes (LEDs) have become the major elements in solid-state lighting, and because of their high luminescence efficiency, these LEDs are potential replacements for traditional lighting sources. However, as injection current increases, the quantum efficiency of InGaN/GaN LEDs decreases; this is the so-called "efficiency droop" phenomenon that has become crucial in high-power operations. The causes of efficiency droop remain intensively debated. For example, electron overflow,[1] nonuniform carrier distribution,[2] and Auger nonradiative recombination[3] have been investigated as the possible reasons for efficiency droop. Several studies have suggested that the absence of polarization fields in InGaN multiple quantum wells (MQWs) can reduce efficiency droop at high injection currents by using polarization-matched AlInGaN MQWs,[4,5] or by adopting nonpolar and semipolar growth directions.[6,7] The polarization field can be eliminated in the active region to restrain the electron current leakage and to enhance the uniformity of hole distribution throughout an active region. However, the growth of quaternary $Al_xGa_{1-x-y}In_yN$ limits the maximum incorporation of indium content into the alloy,[8–10] and the growth of nonpolar or semipolar GaN-based MQWs remains hindered by the existence of high threading dislocation density and basal stacking faults along the c-direction.[11,12] Recently, several research groups have proposed that the efficiency droop can be suppressed by intricately designing the active region; for example, the graded thickness of multiple quantum barriers or wells has led to the improvement of electron overflow and hole transportation.[13–15] The graded composition of multiple quantum barriers or the electron blocking layer can enable the enhancement of hole injection and uniform carrier distribution for effectively increasing the recombination efficiency at a high current density.[2,16] Moreover, the nonsquare shape of quantum wells has been suggested to mitigate Auger recombination and has been experimentally and theoretically demonstrated to suppress efficiency droop by incorporating staggered MQWs.[17,18]

In this study, we fabricated three different designs of active layers with asymmetric triangular MQWs (AT-MQW) and investigated the LED device performance. Compared with LEDs with regular square quantum wells, the LEDs with the AT-MQW structure exhibited improved electroluminescence (EL) emission efficiency and less severe droop phenomena. In addition, the properties of the LEDs with different quantum well structures were characterized and analyzed using commercially available software: Advanced Physical Models of Semiconductor Devices (APSYS). The AT-MQW structures benefitted from the low Auger recombination rate and the enhanced carrier distribution across the active regions. One of the AT-MQW structures had less influence of the polarization field effect, facilitating the LEDs with this AT-MQW structure in exhibiting high EL efficiency and low droop behavior.

All the samples were grown on c-plane patterned sapphire substrates by using metalorganic chemical vapor deposition. Trimethylgallium (TMG), triethylgallium (TEG), trimethylaluminum (TMA), and trimethylindium (TMI) were used as Group III sources; TEG was used for growing MQWs, and TMG was used for growing n-type and p-type GaN layers. Ammonia (NH_3), silane (SiH_4), and bis(cyclopentadienyl)magnesium (Cp_2Mg) were used as the Group V sources, n-type dopant, and p-type dopant, respectively. The V/III ratio was set as 1000, 18 000, and 5000 for the n-GaN, MQW, and p-GaN layers, respectively. The LED structures comprised a nucleation layer, an undoped GaN layer, an n-type GaN layer followed by MQWs, and a p-type GaN layer on top. To grow the designed band structures for the quantum well, the growth parameters and reactor temperature were tuned specifically for MQWs. Fig. 1(a) shows the growth parameters for one period of the symmetric square

[a)]Author to whom correspondence should be addressed. Electronic mail: timtclu@mail.nctu.edu.tw.

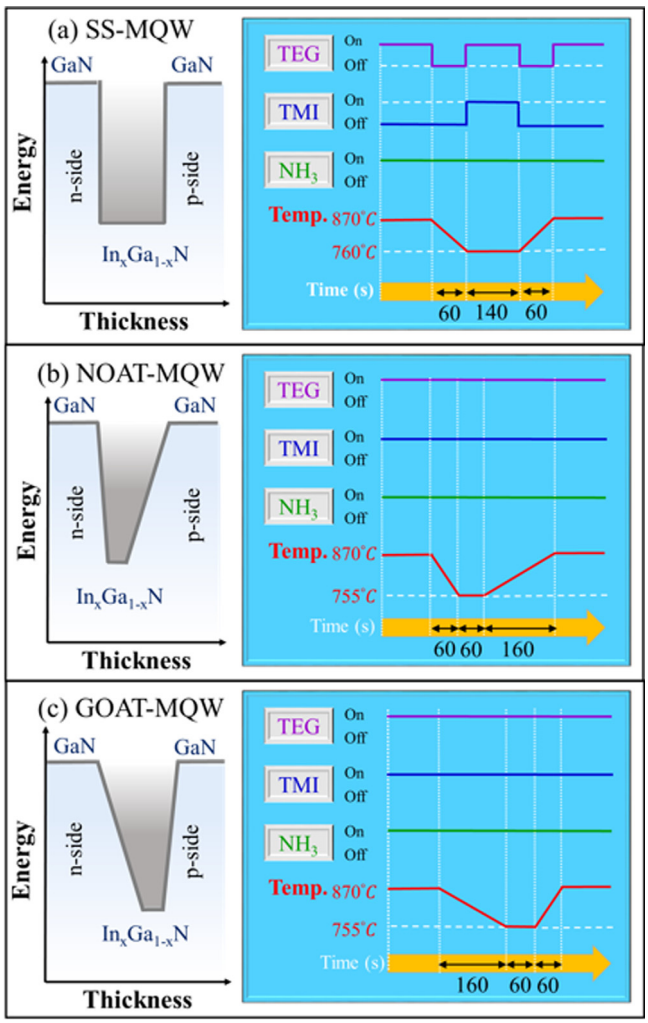

FIG. 1. The schematic representation of quantum well structures and epitaxial growth conditions for (a) SS-MQW, (b) NOAT-MQW, and (c) GOAT-MQW.

MQWs (SS-MQW). The GaN quantum barrier was grown at 870 °C, and the reactor temperature was then reduced to 760 °C for growing the InGaN quantum well while the TMI source was turned on for 140 s. The TMI source was then turned off, and the reactor temperature was increased to 870 °C for growing the subsequent GaN quantum barrier. Figs. 1(b) and 1(c) show the growth parameters for one period of the AT-MQW. Unlike the growth condition used in the symmetric square MQWs, the TMI source was turned on for the entire quantum well period, and the graded indium composition was grown by linearly varying the reactor temperature from 870 °C to 755 °C. To effectively control the quantum well band profile, the growth rate of the AT-MQW was 60% slower than that of the symmetric square quantum well. In Fig. 1(b), the decreasing temperature period lasted 60 s, and the temperature was subsequently maintained at 755 °C for 60 s, and the increasing temperature period lasted 160 s to complete one asymmetric quantum well-inclined toward the gallium face orientation, hereafter referred to as the gallium face-oriented inclination AT-MQW (GOAT-MQW). By contrast, Fig. 1(c) shows that the decreasing temperature period lasted 160 s, and the temperature was then maintained at 755 °C for 60 s, and the increasing temperature period lasted 60 s to complete one asymmetric quantum well-inclined toward the nitrogen face orientation, hereafter referred to as the nitrogen face-oriented inclination AT-MQWs (NOAT-MQW). The GaN quantum barriers were maintained at 12 nm, and the photoluminescence (PL) spectra revealed similar peak positions at 455 nm for these three structures. The surface morphology and crystal quality were investigated using atomic force microscopy, Raman spectroscopy, and X-ray diffraction measurement (data not shown here), and the results did not yield significant differences. The three as-grown samples (the SS-MQW, GOAT-MQW, and NOAT-MQW structures) were then sent for chip processing. The chip dimension was $250 \times 580\ \mu m^2$, and the p-contact was combined with an indium–tin–oxide transparent layer and a finger-shaped metal alloy. Both the p- and n-metal alloys were composed of Cr/Al/Cr/Au layers deposited using an e-gun system. Finally, the chips were tested under a continuous wave current injection at room temperature, and the EL emission was detected by the integrating sphere.

The optical properties of the MQWs were investigated using a power-dependent PL measurement at low and room temperature, excited by a 400 nm laser light, second-harmonically generated using a Ti-sapphire pulse laser (Mira 900), to determine the internal quantum efficiency (IQE). The maximum PL quantum efficiency of a certain excitation condition at low temperature can be normalized to 100%. The IQE measurement results for the MQWs are summarized and plotted as a function of the excitation power in Fig. 2(a). We used AT-MQW to represent both NOAT-MQW and GOAT-MQW because they exhibited similar quantum well shapes and similar IQE values. Moreover, the IQE of SS-MQW was lower. According to the IQE measurement results, we could fit the coefficients of the Shockley–Read–Hall recombination (A) and Auger recombination (C).[19] The A coefficients for the SS-MQW and AT-MQW were $2.5 \times 10^7\ s^{-1}$ and $1.6 \times 10^7\ s^{-1}$, respectively, and the C coefficients for the SS-MQW and AT-MQW were estimated to be approximately $3.0 \times 10^{-30}\ cm^6\ s^{-1}$ and $1.5 \times 10^{-30}\ cm^6\ s^{-1}$, respectively. The AT-MQW exhibited a small Shockley–Read–Hall nonradiative recombination coefficient, which might be an indication of a small number of dislocation centers in the MQWs and superior material quality because of the growth mode. In addition, the small Auger recombination coefficient in the AT-MQW was in good agreement with the theoretical prediction because of the suppression of the large momentum Fourier components in the wave functions of the bound carriers in the AT-MQW structure.[17]

Figs. 2(b) and 2(c) present the output power and normalized efficiency of the SS-MQW, NOAT-MQW, and GOAT-MQW LEDs as a function of the current density. The light output power of NOAT-MQW and GOAT-MQW LEDs were observed to be increased by 11.4% and 24.3% at a current density of $69\ A/cm^2$ (122.7 mW and 136.8 mW vs. 110.1 mW), respectively, compared with the SS-MQW LED, whereas the forward voltage values for the three structures were similar. In addition, the external quantum efficiency (EQE) at a current density of $13.8\ A/cm^2$ for the SS-MQW, NOAT- MQW, and GOAT-MQW LEDs were estimated as 59.6%, 66.5%, and 68.3%, respectively. Therefore, the

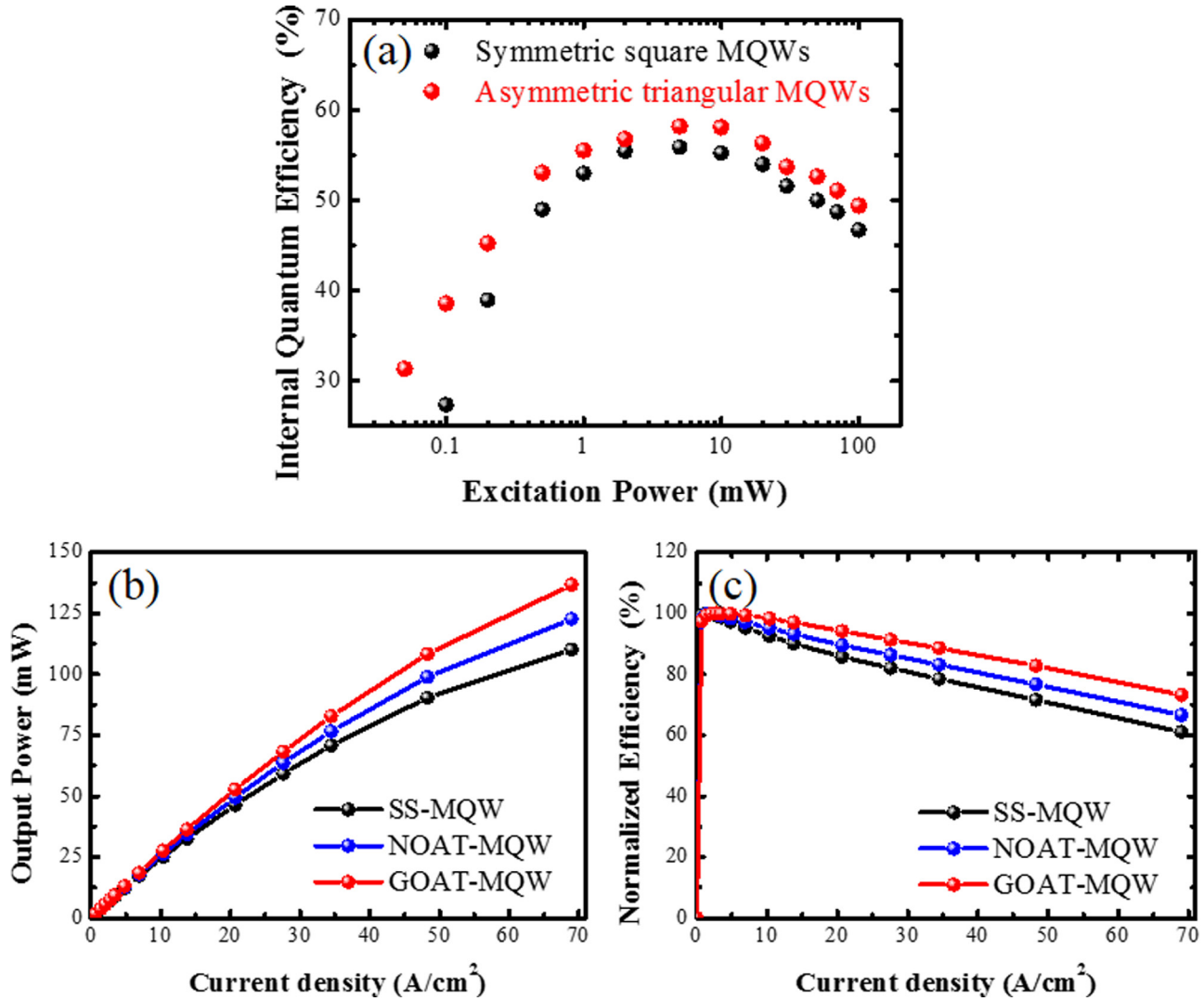

FIG. 2. (a) The IQE of MQWs as a function of the excitation power at 300 K for SS-MQW and AT-MQW. (b) The experimental output power and (c) the normalized efficiency as a function of current density for the SS-MQW, NOAT-MQW, and GOAT-MQW LEDs. The chip dimension was $250 \times 580\ \mu m^2$ and was tested under the continuous wave current injection at room temperature, and the EL emission was detected using the integrating sphere.

power value was also increased by 5.8% and 11.7% at 13.8 A/cm^2 in the NOAT-MQW and GOAT-MQW LEDs, respectively. Among these LED types, the GOAT-MQW LED exhibited the highest efficiency and lowest efficiency droop. The efficiency droop was reduced from 39% for the SS-MQW LED to 27% for the GOAT-MQW LED at 100 mA (corresponding to a current density of 69 A/cm^2), and the peak efficiency current shifted from 1.38 A/cm^2 for the SS-MQW LED to 3.5 A/cm^2 for the GOAT-MQW LED.

Compared with the IQE measurement results, the EL efficiency curves deviated in the GOAT-MQW and NOAT-MQW LEDs, and the deviation became more significant when the injection current was higher. To understand the mechanism of EL efficiency, we used the APSYS simulation tool to consider several crucial factors, including polarization charge, carrier transport, and distribution. We also included the A and C coefficients obtained in the IQE measurement in the simulation model. Fig. 3(a) illustrates the simulated quantum well shape and electron and hole concentration profiles of the SS-MQW, NOAT-MQW, and GOAT-MQW under bias. The electron and hole concentration reflected the wave function distribution in the quantum well. Clearly, the separated spatial distribution of electron and hole envelope functions can be easily observed in the SS-MQWs because of the internal polarization fields caused by the quantum confined stark effect (QCSE) notoriously observed in c-plane InGaN MQWs. Moreover, the electron and hole wave functions of the GOAT-MQWs were closely integrated to enhance the overlap integration facilitated by the triangular quantum wells.[20] Fig. 3(b) presents the band profile and the Fermi energy under bias of the SS-MQW, NOAT-MQW, and GOAT-MQW LEDs. These band profiles and Fermi energy levels in turn influenced the carrier distribution and recombination rates in the MQWs.

Fig. 4(a) shows the radiative recombination rate distributions in the MQWs calculated for different MQW structure designs. For the SS-MQW, the highest radiative recombination rate clearly occurred in the final quantum well nearest to the p-side, and the recombination rate then decreased toward the n-side because of the nonuniform carrier distribution caused by the poor hole transportation in MQWs and the high electron mobility that easily forms the accumulation of carriers in the final quantum well nearest to

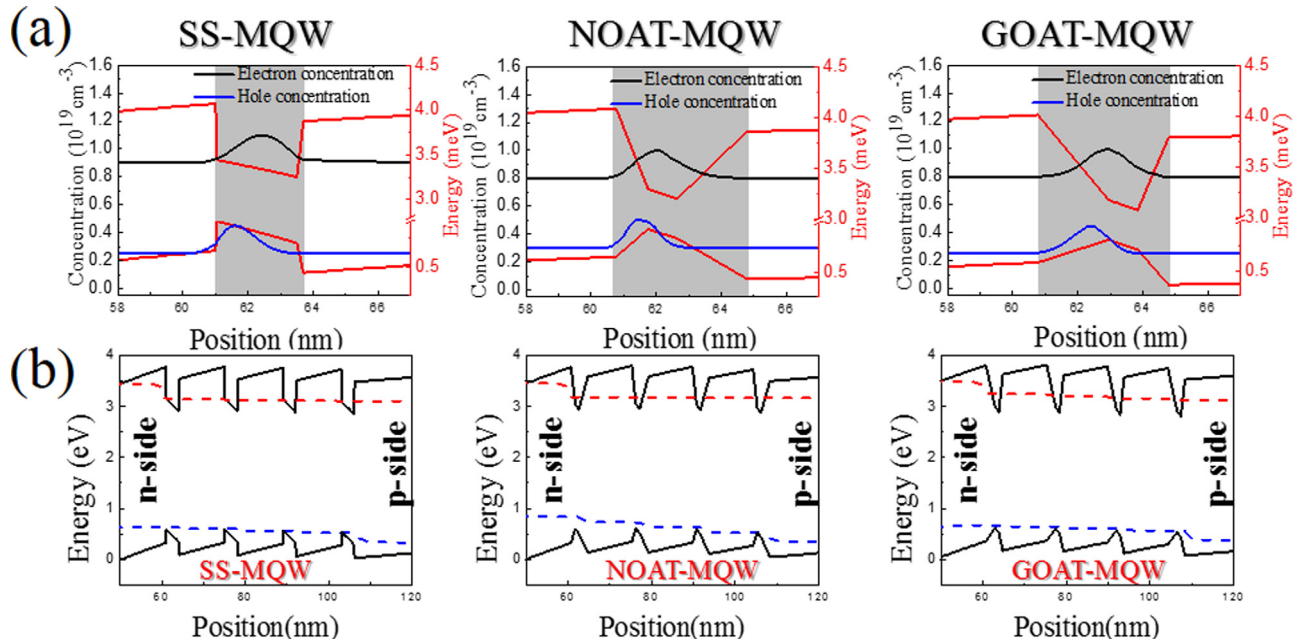

FIG. 3. (a) The simulated quantum well shape and electron and hole concentration of the SS-MQW, NOAT-MQW, and GOAT-MQW. The thickness of one SS-MQW was 2.7 nm with an indium composition of approximately 0.22. The thickness of one AT-MQW was set as 3.5 nm, and the indium composition was 0.25. The thickness of the steep side, bottom, and inclined side of the quantum well were set as 0.6, 1.1, and 1.8 nm, respectively, with the indium composition ranging from 0 to 0.25. (b) The band profile under bias and Fermi energy of the SS-MQW, NOAT-MQW, and GOAT-MQW LEDs.

the p-side. Regarding the NOAT-MQW, the carrier distribution was also nonuniform. The electron tended to move rapidly in the quantum wells toward the p-side because of the inclination for nitrogen face-orientation of AT-MQW, which resulted in the extremely nonuniform distribution of radiative recombination rates. Nevertheless, the higher EL efficiency and lower efficiency droop compared with those of the SS-MQW structure in our experiment can be attributed to the fact that AT-MQW can help reduce the effects of Auger recombination and decrease nonradiative efficiency. Furthermore, the radiative recombination rate distribution of the GOAT-MQW was entirely different from those of the other MQW structures, exhibiting the most uniform radiative recombination rate distribution among the MQWs. The graded barrier band profile of the GOAT-MQW enhanced the carrier distribution. Therefore, the GOAT-MQW structure can achieve the highest external quantum efficiency among the three structures.

We further investigated the influence of the polarization fields on the efficiency droop by changing the polarization charge amount in the simulation for the SS-MQW and GOAT-MQW structures, as shown in Fig. 4(b). The efficiency droop of SS-MQW was severe when the polarization field (approximately 30%) was turned on because of the reduction of the radiative recombination under the influence of QCSE. The efficiency improved when the polarization field was turned off for the SS-MQW structure. However, the efficiency droop phenomenon remained obvious because of other contributing factors, such as the aforementioned carrier overflow and nonuniform carrier distribution. The droop

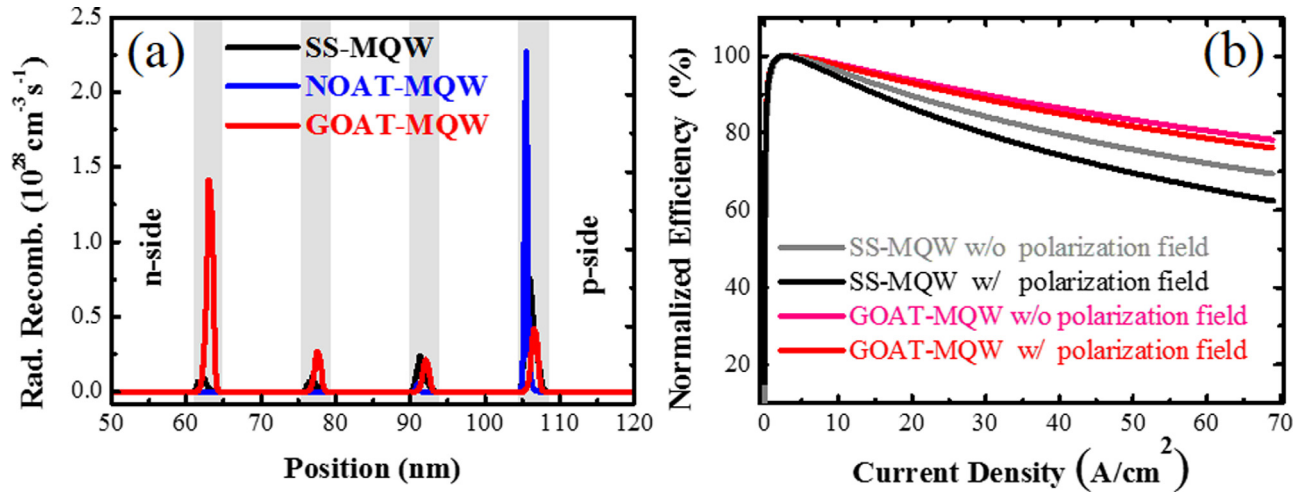

FIG. 4. (a) The simulated radiative recombination rates in the MQWs of the SS-MQW, NOAT-MQW, and GOAT-MQW LEDs. (b) The simulated normalized efficiency as functions of current density with and without the polarization fields for the SS-MQW and GOAT-MQW LEDs.

efficiency of GOAT-MQW structures were mitigated regardless of whether the polarization field was turned on or off. When the influence of the polarization field was applied to the SS-MQW, the energy band in the quantum well bent toward the gallium face. It was intuitive to compensate for the energy band bending by applying the NOAT-MQW structure. Nevertheless, the experiment results indicated that the NOAT-MQW remained affected by the efficiency droop. Thus, in this study, we applied the GOAT-MQW structure so that the slopes of the triangular quantum wells were in the reverse direction of the polarization fields. By implementing this structure, the effects of the polarization fields on the InGaN MQWs were effectively suppressed to minimize the resulting efficiency droop. The simulation results were in good agreement with the experimental results, indicating that using GOAT-MQW enhanced the performance of the InGaN LEDs, particularly regarding high current injection operation.

In summary, we fabricated and analyzed three quantum well structures for LEDs. The light output powers of the SS-MQW, NOAT-MQW, and GOAT-MQW LEDs were, respectively, measured as 110.1 mW, 122.7 mW, and 136.8 mW at 100 mA (corresponding to a current density of 69 A/cm^2). Furthermore, the EQE at 20 mA for the SS-MQW, NOAT-MQW, and GOAT-MQW LEDs were estimated to be 52.8%, 56.1%, and 60.0%, respectively. The efficiency droop was reduced from 39% for the SS-MQW LED to 27% for the GOAT-MQW LED at a current density of 69 A/cm^2. The GOAT-MQW LED likely exhibited high EL efficiency and low efficiency droop because of the lower Auger recombination rate, improved carrier distribution, and reduced influence of polarization fields in the triangular quantum wells than in the square quantum wells. We believe that this InGaN MQW design is a simple and cost-effective method suitable for applications in high-power light emitting sources.

We acknowledge the help of Prof. S. C. Wang and Prof. H. C. Kuo at National Chiao Tung University for contributing fruitful discussions and technical support. This work was partially supported by EPISTAR Corporation for Industry-university Collaboration project, by the Ministry of Education Aim for the Top University program and by the National Science Council of Taiwan under Contract No. NSC100-2628-E009-013-MY3.

[1]K. J. Vampola, M. Iza, S. Keller, S. P. DenBaars, and S. Nakamura, Appl. Phys. Lett. **94**, 061116 (2009).
[2]C. H. Wang, S. P. Chang, P. H. Ku, J. C. Li, Y. P. Lan, C. C. Lin, H. C. Yang, H. C. Kuo, T. C. Lu, S. C. Wang, and C. Y. Chang, Appl. Phys. Lett. **99**, 171106 (2011).
[3]A. David and M. J. Grundmann, Appl. Phys. Lett. **96**, 103504 (2010).
[4]M.-H. Kim, M. F. Schubert, Q. Dai, J. K. Kim, E. F. Schubert, J. Piprek, and Y. Park, Appl. Phys. Lett. **91**, 183507 (2007).
[5]M. F. Schubert, J. Xu, J. K. Kim, E. F. Schubert, M. H. Kim, S. Yoon, S. M. Lee, C. Sone, T. Sakong, and Y. Park, Appl. Phys. Lett. **93**, 041102 (2008).
[6]S. P. Chang, T. C. Lu, L. F. Zhuo, C. Y. Jang, D. W. Lin, H. C. Yang, H. C. Kuo, and S. C. Wang, J. Electrochem. Soc. **157**, H501–H503 (2010).
[7]S. C. Ling, T. C. Lu, S. P. Chang, J. R. Chen, H. C. Kuo, and S. C. Wang, Appl. Phys. Lett. **96**, 231101 (2010).
[8]A. Cremades, V. Navarro, J. Piqueras, A. Lima, O. Ambacher, and M. Stutzmann, J. Appl. Phys. **90**, 4868 (2001).
[9]J. Huang, X. Dong, X. Luo, D. Li, X. Liu, Z. Xu, and W. Ge, J. Cryst. Growth **247**, 84 (2003).
[10]E. Monroy, N. Gogneau, D. Jalabert, E. Bellet-Amalric, Y. Hori, F. Enjalbert, L. S. Dang, and B. Daudin, Appl. Phys. Lett. **82**, 2242–2244 (2003).
[11]M. Craven, S. Lim, F. Wu, J. Speck, and S. DenBaars, Appl. Phys. Lett. **81**, 469 (2002).
[12]H. M. Huang, C. Y. Chang, T. C. Lu, and C. C. Yang, J. Electrochem. Soc. **158**, H915 (2011).
[13]J. P. Liu, J. H. Ryou, R. D. Dupuis, J. Han, G. D. Shen, and H. B. Wang, Appl. Phys. Lett. **93**, 021102 (2008).
[14]C. H. Wang, S. P. Chang, W. T. Chang, J. C. Li, Y. S. Lu, Z. Y. Li, H. C. Yang, H. C. Kuo, T. C. Lu, and S. C. Wang, Appl. Phys. Lett. **97**, 181101 (2010).
[15]Z. G. Ju, W. Liu, Z.-H. Zhang, S. T. Tan, Y. Ji, Z. B. Kyaw, X. L. Zhang, S. P. Lu, Y. P. Zhang, B. B. Zhu, N. Hasanov, X. W. Sun, and H. V. Demir, Appl. Phys. Lett. **102**, 243504 (2013).
[16]C. H. Wang, C. C. Ke, C. Y. Lee, S. P. Chang, W. T. Chang, J. C. Li, Z. Y. Li, H. C. Yang, H. C. Kuo, T. C. Lu, and S. C. Wang, Appl. Phys. Lett. **97**, 261103 (2010).
[17]R. Vaxenburg, E. Lifshitz, and A. L. Efros, Appl. Phys. Lett. **102**, 031120 (2013).
[18]H. Zhao, G. Liu, X. H. Li, G. S. Huang, J. D. Poplawsky, S. T. Penn, V. Dierolf, and N. Tansu, Appl. Phys. Lett. **95**, 061104 (2009).
[19]X. Ni, J. Lee, M. Wu, X. Li, R. Shimada, and Ü. Özgür, A. A. Baski, H. Morkoç, T. Paskova, G. Mulholland, and K. R. Evans, Appl. Phys. Lett. **95**, 101106 (2009).
[20]H. Zhao, G. Liu, J. Zhang, J. D. Poplawsky, V. Dierolf, and N. Tansu, Opt. Express **19**, A991 (2011).